

Robust-Wide: Robust Watermarking against Instruction-driven Image Editing

Runyi Hu¹, Jie Zhang², Tianwei Zhang², Jiwei Li¹

¹Zhejiang University, ²Nanyang Technological University

{runyi_hu, jiwei_li}@zju.edu.cn

{jie_zhang, tianwei.zhang}@ntu.edu.sg

Abstract

Instruction-driven image editing allows users to quickly edit an image according to text instructions in a forward pass. Nevertheless, malicious users can easily exploit this technique to create fake images, which could cause a crisis of trust and harm the rights of the original image owners. Watermarking is a common solution to trace such malicious behavior. Unfortunately, instruction-driven image editing can significantly change the watermarked image at the semantic level, making it less robust and effective.

We propose Robust-Wide, the first robust watermarking methodology against instruction-driven image editing. Specifically, we adopt the widely-used encoder-decoder framework for watermark embedding and extraction. To achieve robustness against semantic distortions, we introduce a novel Partial Instruction-driven Denoising Sampling Guidance (PIDSG) module, which consists of a large variety of instruction injections and substantial modifications of images at different semantic levels. With PIDSG, the encoder tends to embed the watermark into more robust and semantic-aware areas, which remains in existence even after severe image editing. Experiments demonstrate that Robust-Wide can effectively extract the watermark from the edited image with a low bit error rate of nearly 2.6% for 64-bit watermark messages. Meanwhile, it only induces a neglectable influence on the visual quality and editability of the original images. Moreover, Robust-Wide holds general robustness against different sampling configurations and other image editing methods such as ControlNet-InstructPix2Pix, MagicBrush, Inpainting and DDIM Inversion.

1. Introduction

Recently released Text-to-Image (T2I) diffusion models (e.g., GLIDE [1], DALL.E 2 [2], Imagen [3], Stable Diffusion [4]) have pushed image generation capabilities to a new level. Trained on massive text-image pairs collected from the Internet, these models can generate high-quality photo-realistic images based on given text prompts. Instruction-

driven image editing, a fantastic technique utilizing the power of T2I diffusion models, can edit the images on demand according to the instructions. Different models have been introduced to achieve this task. For instance, InstructPix2Pix [5] is a popular instruction-driven image editing model, which is fine-tuned from Stable Diffusion [4] on the dataset generated by GPT-3 [6] and Prompt2Prompt [7]. Afterwards, HIVE [8], MagicBrush [9], and MGIE [10] are proposed to improve InstructPix2Pix.

Despite the success of the instruction-driven image editing technique, these models could be misused by malicious users. First, attackers can exploit these models to modify normal images to create fake news, causing a crisis of trust in an individual or even a country. Typical examples include changing someone’s face or expression, forging endorsements for commercial gain, or taking off the clothes to produce vulgar images. Second, attackers can migrate the style based on a certain painting or make local modifications while keeping the basic composition of the painting unchanged to create new works, which shall be confirmed as plagiarism, infringing the IP rights of the work’s owner. By integrating the personalization technique (e.g., Textual Inversion [11]), they may compose some concepts learned from other images in the edited image, which will undoubtedly lead to wider infringement on the concept’s owners.

To identify such misuse and trace malicious users, a common approach is watermarking. We can embed a secret watermark message into the original image, which can be extracted later for ownership verification. The embedded watermark must be robust enough against various distortions. Traditional robust watermarking strategies [12] mainly embed the watermark into a transformed domain to resist spatial distortions. To achieve robustness against more complex digital distortions, some deep watermarking methods are further proposed, e.g., HiDDeN [13] and MBRS [14]. Additionally, researchers also introduced new methods to pursue robustness against physical distortions, including StegaStamp [15] and PIMoG [16]. Unfortunately, all the above solutions mainly target the pixel-level distortions, and fail to resist instruction-driven image editing,

which induces significant distortions in the semantic level.

To remedy this issue, we propose Robust-Wide, the first robust watermarking method for instruction-driven image editing. We are motivated by the popular encoder-noise layer-decoder framework in most deep watermarking methods [13–16], which jointly achieve watermark embedding and extraction in an end-to-end way and leveragzhi lie the noise layer to simulate specific distortions to obtain the corresponding robustness. However, the main challenge in our task is how to simulate the distortions caused by instruction-driven image editing. To this end, we design a novel Partial Instruction-driven Denoising Sampling Guidance (*PIDSG*) module in Robust-Wide. Briefly, *PIDSG* allows the gradient of the last k sampling steps to flow into the training pipeline, making the non-differentiable sampling process trainable. Additionally, it injects diverse instructions to guide distortions, forcing the encoder and decoder to focus on semantic areas for watermark embedding and extraction.

We perform extensive experiments to demonstrate the robustness of Robust-Wide during the instruction-driven image editing process. It achieves a low Bit Error Rate (BER) of nearly 2.6% for 64-bit watermark messages, while preserving the visual quality and editability of original images. Besides the robustness against semantic distortions, Robust-Wide acquires inherent robustness against pixel-level distortions such as JPEG and color shifting, which are unseen during training. It also holds general robustness against different sampling configurations and models.

2. Background

2.1. Diffusion Model

Inspired by the non-equilibrium statistical physics, Diffusion Model (DM) [17] destroys the structure in a data distribution through an iterative forward diffusion process, and learns a reverse diffusion process to restore data's structure. Denoising Diffusion Probabilistic Model (DDPM) [18] further improves the performance of DM by training on a weighted variational bound with the following objective:

$$L_{DM} = \mathbb{E}_{x, \epsilon \sim \mathcal{N}(0,1), t} \left[\|\epsilon - \epsilon_\theta(x_t, t)\|_2^2 \right], \quad (1)$$

where x is the input image, ϵ is the randomly sampled Gaussian noise, $t \in \{1, \dots, T\}$ is the uniformly sampled timestep, x_t is the noisy version of x , and ϵ_θ is the diffusion model trained to predict a denoised variant of x_t .

Many T2I diffusion models, e.g., GLIDE [1], DALL·E 2 [2] and Imagen [3] are based on DDPM. They operate directly in the pixel space, which can consume a large amount of computational resources for both training and evaluation. To overcome these shortcomings, Latent Diffusion Model (LDM) [4] is proposed to perform the noise and denoise

process in the latent space of the pre-trained VAE:

$$L_{LDM} = \mathbb{E}_{\mathcal{E}(x), \epsilon \sim \mathcal{N}(0,1), t} \left[\|\epsilon - \epsilon_\theta(z_t, t)\|_2^2 \right], \quad (2)$$

where \mathcal{E} is the encoder of VAE and z_t is the noisy latent variable. Stable Diffusion is a popular T2I model based on LDM with great impact and outstanding performance.

2.2. Instruction-driven Image Editing

There are mainly five popular instruction-driven image editing models, which are all based on DMs. (1) InstructPix2Pix [5] performs editing in a forward pass quickly and does not require any user-drawn mask, additional images, per-example fine-tuning, or inversion. It is trained in an end-to-end manner, with the dataset generated by GPT-3 [6] and Prompt2Prompt [7]. Each item in the dataset contains a source image, an editing instruction, and a subsequent edited image. During training, the image and instruction are regarded as conditions c_I and c_T , respectively, while the edited image is the ground-truth output. Therefore, the training object is as follows:

$$L = \mathbb{E}_{\mathcal{E}(x), \mathcal{E}(c_I), c_T, \epsilon \sim \mathcal{N}(0,1), t} \left[\|\epsilon - \epsilon_\theta(z_t, t, \mathcal{E}(c_I), c_T)\|_2^2 \right]. \quad (3)$$

(2) ControlNet [19] is a dedicated framework that amplifies the capability and controllability of pre-trained T2I diffusion models by integrating spatial conditioning controls. Therefore, we can regard original images as spatial conditioning controls and train ControlNet on the dataset of InstructPix2Pix to realize instruction-driven image editing, which is called ControlNet-InstructPix2Pix [19]. (3) Afterwards, HIVE [8] improves InstructPix2Pix by harnessing human feedback to tackle the misalignment between editing instructions and resulting edited images. (4) MagicBrush [9] introduces the first large-scale and manually annotated dataset for instruction-guided real image editing and fine-tunes InstructPix2Pix on the dataset for better performance. (5) MGIE [10] uses multimodal large language models to derive expressive instructions and provide explicit guidance to further improve the editing performance while maintaining the efficiency.

In this paper, we mainly target InstructPix2Pix, and assess the generalization of our method to ControlNet-InstructPix2Pix and MagicBrush, since these models are open-sourced and publicly available.

2.3. Robust Watermarking

Robust watermarking is widely used for IP protection and forensics. Traditional methods (e.g., DWT-DCT [12] and DWT-DCT-SVD [12]) embed a pre-defined watermark message into transformed domains to achieve simple robustness against different operations, e.g., affine transformation, scaling, etc. HiDDeN [13] is the first to leverage deep neural networks for watermark embedding and extraction. Importantly, it simulates JPEG compression into a

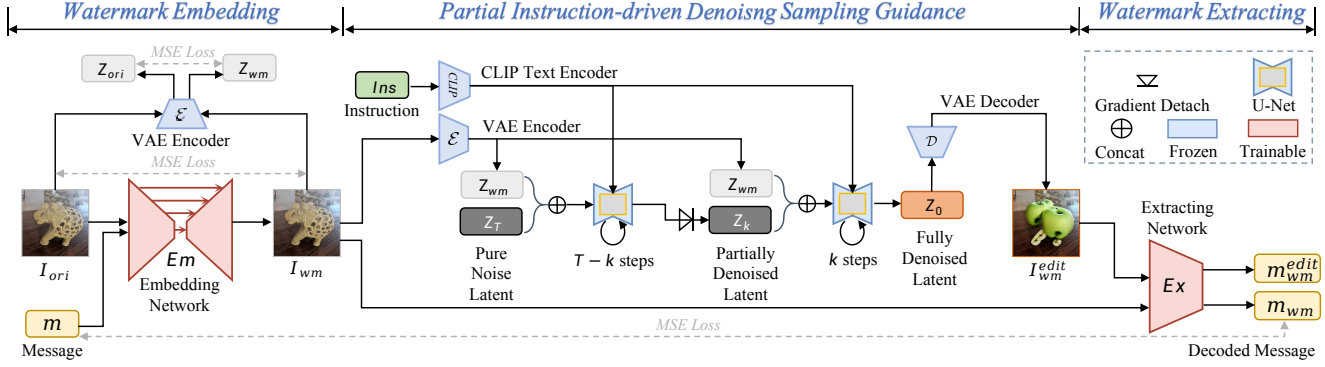


Figure 1. The overall training pipeline of Robust-Wide.

differential module, inserted into the famous encoder-noise layer-decoder framework for robustness enhancement. RivaGAN [20] applies a customized attention-based mechanism to embed diverse data and includes a separate adversarial networks for optimizing robustness. Afterwards, MBRS [14] utilizes a mixture of real JPEG, simulated JPEG, and noise-free images to get superior robustness performance against JPEG compression, which is also robust to various digital distortions. In addition to digital robustness, numerous works (LFM [21], StegaStamp [15], RIHOOP [22], PIMoG [16]) try to acquire robustness against physical operations such as screen-shooting, print-shooting, etc. However, none of them can resist instruction-driven image editing, which belongs to digital distortions.

In this paper, we compare our method with MBRS [14], the state-of-the-art digital-robust watermarking method. Furthermore, we adopt DWT-DCT [12], DWT-DCT-SVD [12], and RivaGAN [20] as the baseline methods, which are suggested by Stable Diffusion’s official webpage [23].

3. Methodology

3.1. Overview

We introduce Robust-Wide, a novel methodology to embed robust watermarks into images, which can resist instruction-driven editing. Its overall training pipeline is shown in Figure 1. An embedding network E_m and extracting network E_x are jointly trained to achieve watermark embedding and extraction, respectively. Furthermore, a novel Partial Instruction-driven Denoising Sampling Guidance (PIDSG) module is integrated into the pipeline to enhance the watermark robustness against instruction-driven image editing. With the trained networks, we can use E_m to embed a secret watermark message into a protected image, and release it to public. If a malicious user performs instruction-driven image editing over this watermarked image without authorization, we are able to detect this misuse by using E_x to extract the watermark message from the

edited image. Below we describe each step in detail.

3.2. Watermark Embedding

An embedding network E_m is introduced to generate a watermarked image I_wm from the original image I_{ori} , where the watermark is a random L -bit message $m \in \{0, 1\}^L$. Specifically, we adopt U-Net [24] as the structure of E_m . To match m with the dimension of I_{ori} , E_m converts the flattened version of m in the shape of $1 \times \sqrt{L} \times \sqrt{L}$ to the shape of $C \times H \times W$ using some transposed convolutional layers, where C is the predefined feature channel, H and W are the height and weight of I_{ori} . Then, we concatenate the reshaped message with I_{ori} . To preserve the editing capability of the image, I_wm should be visually consistent with I_{ori} . We first adopt the L_2 distance between I_{ori} and I_wm in the pixel level, *i.e.*,

$$L_{em_1} = L_2(I_{ori}, I_wm) = L_2(I_{ori}, E_m(I_{ori}, m)). \quad (4)$$

Furthermore, we add another constraint between I_{ori} and I_wm in the feature space, represented by the encoder \mathcal{E} of VAE in InstructPix2Pix, *i.e.*,

$$L_{em_2} = L_2(Z_{ori}, Z_{wm}) = L_2(\mathcal{E}(I_{ori}), \mathcal{E}(I_wm)). \quad (5)$$

3.3. Partial Instruction-driven Denoising Sampling Guidance (PIDSG)

Existing watermarking solutions mainly consider the robustness against pixel-level distortions. In contrast, instruction-driven image editing changes an image significantly at the semantic level, making these approaches ineffective. We note that instruction-driven image editing involves the injection of a large number of different semantic instructions and varying degrees of image modifications at different semantic levels, which can be utilized to guide the robust and semantic-aware watermark embedding and extraction process. Thus, our intuitive idea is to incorporate the editing process into the end-to-end training framework. However, one challenge is that during the denoising

sampling process of InstructPix2Pix, gradients are not allowed to flow directly. Introducing this process into training would result in the inability of gradients to propagate from the watermark decoder through the sampling process back to the watermark encoder. In other words, this would lead to a discontinuity in the computational graph, rendering the entire process non-differentiable. While a straightforward approach might be to open gradients for the numerous denoising sampling steps, this would introduce a significant memory overhead. To address this, we design the Partial Instruction-driven Denoising Sampling Guidance (*PIDSG*) module, which selectively allows gradients to flow only in the last k sampling steps. This design not only makes the entire method feasible but also enables the process to be differentiable and amenable to end-to-end optimization.

As shown in the middle part of Figure 1, InstructPix2Pix consists of VAE [25], U-Net [24], and CLIP text encoder [26]. We freeze all the parameters of these models. During training, the encoder \mathcal{E} of VAE converts I_{wm} to its latent $Z_{wm} = \mathcal{E}(I_{wm})$. Then, Z_{wm} is concatenated with the pure noise latent Z_T and sent to U-Net to perform denoising sampling iterations. Assuming the sampling process totally has T steps, we truncate the gradient flow in the first $T - k$ steps to obtain the partially denoised latent Z_k . After that, we concatenate Z_k with Z_{wm} and perform the last k sampling steps (dubbed gradient backward steps) to enable the gradient flow. The CLIP text encoder processes the instruction Ins and outputs the textual embedding to guide the whole sampling process. Finally, after T sampling steps, the fully denoised latent Z_0 is produced and converted to the edited image I_{wm}^{edit} by the decoder \mathcal{D} of VAE.

3.4. Watermark Extracting

For the extracting network E_x , we leverage some residual blocks as its architecture. With the edited image I_{wm}^{edit} , E_x aims to extract the message m_{wm}^{edit} that is consistent to the original embedded message m , *i.e.*,

$$L_{ex_1} = MSE(m, m_{wm}^{edit}) = MSE(m, E_x(I_{wm}^{edit})). \quad (6)$$

For effective forensic, we also require E_x to be capable of extracting the embedded watermark message m_{wm} from the watermarked image I_{wm} before editing:

$$L_{ex_2} = MSE(m, m_{wm}) = MSE(m, E_x(I_{wm})). \quad (7)$$

Interestingly, we observe that the training will not converge without L_{ex_2} . We explain that the extracting network E_x cannot find the watermark area if only fed with edited images that are different from the original images at the semantic level. More results can be found in Sec. 4.5.

3.5. Joint Training

We jointly train E_m and E_x with the above-mentioned components: watermark embedding, *PIDSG*, and water-

mark extraction. The total loss is formulated as follows:

$$L_{total} = L_{em_1} + \lambda_1 L_{em_2} + \lambda_2 L_{ex_1} + \lambda_3 L_{ex_2}, \quad (8)$$

where $\lambda_1 = 0.001$, $\lambda_2 = 0.1$, and $\lambda_3 = 1$ by default are the hyperparameters to balance each loss item. More analysis can be found in Sec. 4.5.

4. Experiments

Datasets. To train the embedding and extracting networks, we adopt 20k image-instruction pairs from the dataset used in InstructPix2Pix. We also select 1.2k additional samples that do not overlap with the above training data for evaluation by default. Besides, we collect some real-world images from the Internet, which cover 6 types (*i.e.*, person, animal, object, architecture, painting, and scenery) and each type has 5 images. Then, we use InstructPix2Pix to edit these images based on 6 instructions and generate 8 images per instruction to finally obtain 1.44k edited images for testing.

Implementation Details. We train all our models on a single A6000 GPU, with a learning rate of 1e-3, batch size of 2, and total steps of 20,000. We use the AdamW optimizer with a cosine scheduler of 400 warm-up steps. Images used for training and evaluation are all 512×512 by default. For the configurations of *PIDSG*, we adopt the Euler sampler, with 20 inference steps, the text guidance scale $s_T=10.0$, and image guidance scale $s_I=1.5$.

We choose four baselines for comparisons, *i.e.*, DWT-DCT [27], DWT-DCT-SVD [27], RivaGAN [20], and MBRS [14]. We directly use their official code for implementation. Noteably, the released model of MBRS only supports 256×256 images with 256 bits.

Metrics. To evaluate the effectiveness of our method, we measure the Bit Error Rate (BER) between the extracted watermark X and ground-truth watermark Y , *i.e.*, $BER(X, Y) = \frac{\sum_{i=1}^L (X_i \neq Y_i)}{L}$, where $X_i, Y_i \in \{0, 1\}$ and L is the watermark length. To assess the fidelity, we adopt PSNR and SSIM to measure the visual quality of watermarked images. To verify how the watermarked image can preserve its original editability, we adopt the CLIP image similarity (CLIP-I) and CLIP Text-Image Direction Similarity (CLIP-T), which are also used in InstructPix2Pix [5].

4.1. Effectiveness Evaluation

Table 1 compares the effectiveness of Robust-Wide with the baseline methods with different image sizes and watermark lengths. For Robust-Wide, we consider the implementation without and with *PIDSG*. From this table, it is obvious that none of the baseline methods can resist instruction-driven image editing, with the BER of around 50%. Comparably, Robust-Wide is effective with a low BER of 2.6579% in 1.2k InstructPix2Pix samples and

Method	Image Size	Watermark Length (bits)	BER (%) ↓		PSNR↑	SSIM↑
			w/o. Editing	w/. Editing		
DWT-DCT [12]	512x512	32	11.9351	49.2286	38.7123	0.9660
DWT-DCT-SVD [12]	512x512	32	0.0314	47.5680	38.6488	0.9726
RivaGAN [20]	512x512	32	0.6276	40.5256	40.6132	0.9718
MBRS [14]	256x256	256	0.0000	46.7661	43.9780	0.9870
Robust-Wide (w/o. <i>PIDSG</i>)	512x512	64	0.0000	50.1558	55.3710	0.9982
Robust-Wide (w/. <i>PIDSG</i>)	512x512	64	0.0000	2.6579	41.9142	0.9910
Robust-Wide (w/o. <i>PIDSG</i>) †	512x512	64	0.0000	51.0801	55.3715	0.9983
Robust-Wide (w/. <i>PIDSG</i>) †	512x512	64	0.0000	2.6062	41.4038	0.9922

Table 1. Quantitative results compared with other methods. † denotes the results calculated on real-world images.

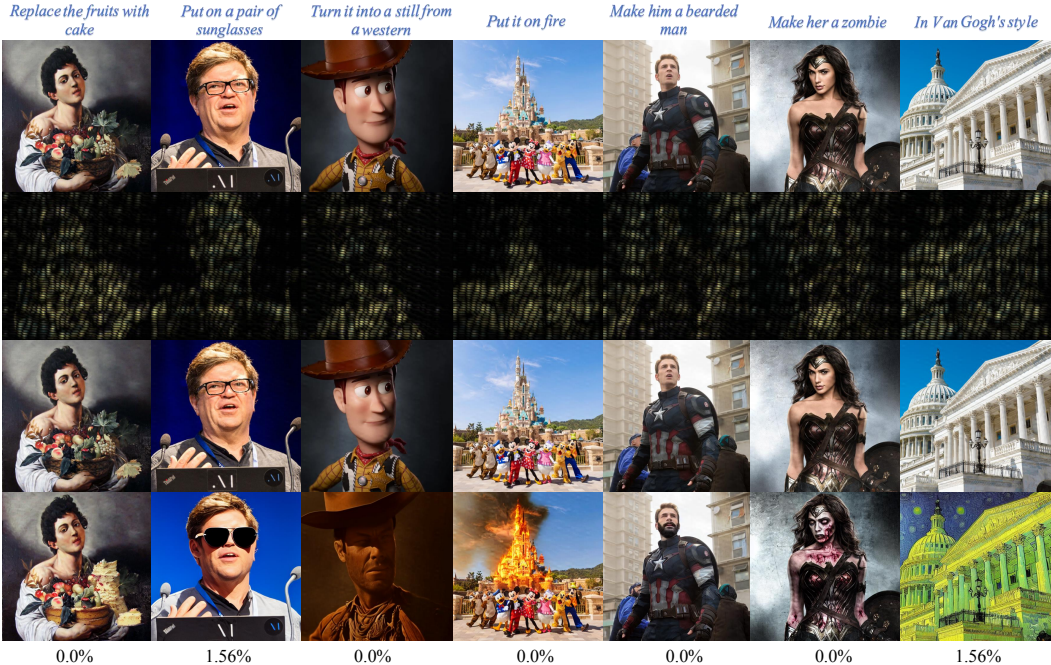


Figure 2. Visual results for Robust-Wide. From top to bottom: instructions, original images, normalized residual images, watermarked images, edited images, and the corresponding BERs.

BER (%)	w/o. Editing	w/. Editing
Original Images	49.8403	48.8550
Watermarked Images	0.0000	2.6579

Table 2. The integrity of Robust-Wide.

Images for Editing	CLIP-I↑	CLIP-T↑
Original Images	0.8402	0.2183
Watermarked Images	0.8430	0.2148

Table 3. The influence of Robust-Wide on the image editability.

2.6062% in 1.44k real-world samples. Importantly, the removal of *PIDSG* leads to a complete failure, revealing the importance of *PIDSG*. Table 2 shows that Robust-Wide will not extract watermarks from original images with or

without editing, guaranteeing forensic integrity.

4.2. Fidelity Evaluation

Table 1 also shows the PSNR and SSIM of different methods. We observe that Robust-Wide can achieve the comparable visual quality with other baseline methods. Table 3 compares the values of CLIP-I and CLIP-T for original and watermarked images. The slight difference indicates that Robust-Wide induces little influence on the editability. Figure 2 shows some visual results using our Robust-Wide, which further confirms the fidelity. Specifically, the normalized residual images are computed as $N(|I_{wm} - I_{ori}|)$, where $N(x) = (x - \min(x)) / (\max(x) - \min(x))$. From these images, it is evident that the watermark is predominantly embedded along the contours of the main subjects (such as people or objects)

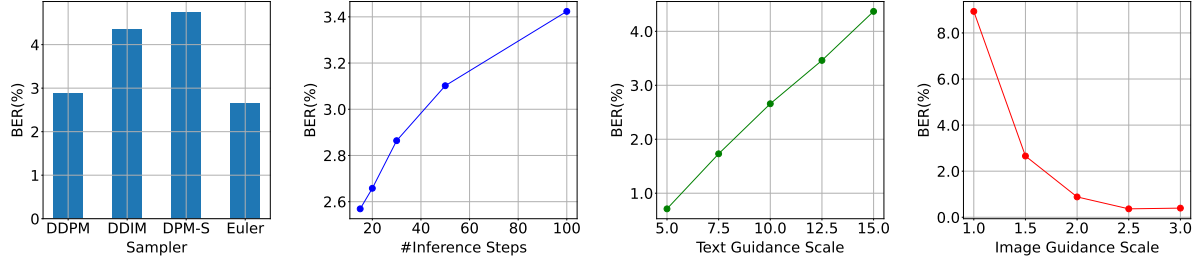


Figure 3. Robustness of Robust-Wide against different diffusion sampling configurations.

and in the background (secondary elements like buildings). We posit that these areas may be robust regions related to conceptual content and therefore Robust-Wide tends to embed watermarks into robust concept-aware areas.

4.3. Robustness Evaluation

Pixel-level Distortions. We apply different pixel-level distortions in three ways: (I) pre-processing watermarked images before editing; (II) post-processing watermarked images; (III) post-processing edited images based on watermarked images. Table 4 shows the extraction error of Robust-Wide against different pixel-level distortion types in three scenarios. It is obvious that Robust-Wide demonstrates strong robustness against these distortions even if we do not involve them during training.

Additionally, we also test Robust-Wide’s robustness against DiffWA[28], a new watermark removal attack. This attack utilizes an image-to-image conditional diffusion model to add noise on the watermarked image and then restores the image while removing the embedded watermark. Due to the unavailability of DiffWA’s source code, we utilize the open-source SDEdit[29] from Diffusers to carry out the process of adding noise and subsequently restoring the watermarked images. We configure the sampling parameters as follows: strength=0.2, prompt=NULL, with all other sampling parameters as their default values. As shown in the “Noise+Denoise” row of Table 4, Robust-Wide is effective in all three situations with $BER < 10\%$.

Different Sampling Configurations. We assess the robustness of Robust-Wide against different diffusion sampling configurations. Figure 3 shows the corresponding results. We have the following observations. (1) Robust-Wide is generally effective for different samplers. (2) As the total number of inference steps increases, the edited images become more fine-grained while the BER slightly increases (within a range of 1%). We explain that more details lead to larger differences between the edited and original images. (3) A larger text guidance scale (s_T) and smaller image guidance scale (s_I) indicate more severe image editing. Robust-Wide achieves BER of below 5% in all cases except when s_I is 1, validating its general robustness in different settings.

Distortion Type	BER(%)↓		
	I	II	III
None	2.6579	0.0000	2.6579
JPEG	2.7256	0.0013	2.7934
Median Blur	2.4926	0.0000	2.9574
Gaussian Blur	2.7074	0.0013	2.8489
Gaussian Noise	3.0672	0.0716	6.0546
Sharpness	2.6150	0.0013	2.7773
Brightness	12.2907	4.0733	9.4796
Contrast	5.1336	0.9210	4.3346
Saturation	3.0455	0.0000	3.0373
Hue	2.7591	0.0000	3.2829
Noise+Denoise	8.6401	3.9071	9.3654

Table 4. Robustness of Robust-Wide against pixel-level distortions in three processing scenarios.

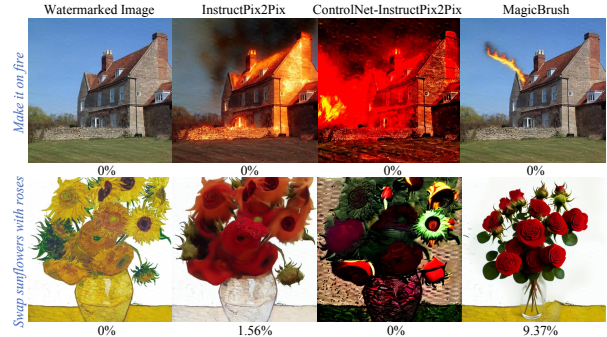


Figure 4. Comparisons of image editing results among InstructPix2Pix, ControlNet-InstructPix2Pix, and MagicBrush.

Other Image Editing Methods. In addition to InstructPix2Pix, we further evaluate our robustness against its extension ControlNet-InstructPix2Pix and MagicBrush on the 1.2k-samples dataset. Experiments show that Robust-Wide can achieve an average BER of 0.96% on ControlNet-InstructPix2Pix and 9.34% on MagicBrush. Figure 4 shows some visual examples. For the instruction “swap sunflowers with roses”, MagicBrush makes the edited image more different from the original image, lead-

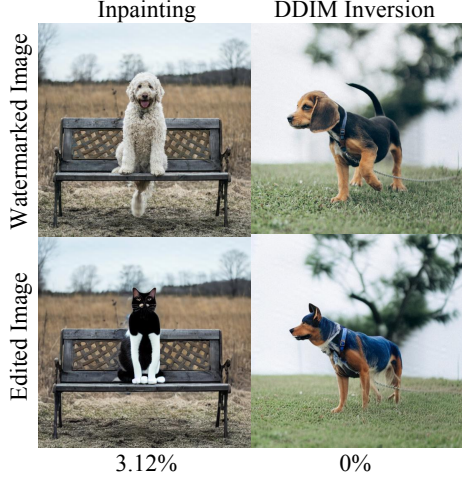


Figure 5. Robustness against Inpainting and DDIM Inversion.

ing to a relatively higher but still acceptable BER.

We also tested the robustness of Robust-Wide against some other popular non-instruction-driven image editing methods, such as Inpainting and DDIM Inversion[30] based on Stable Diffusion Models. We found that, even though Robust-Wide has never seen these image editing methods during training, it still demonstrates effective resistance as shown in Figure 5.

Continual Editing. A user may utilize InstructPix2Pix to perform multiple edits on a single image. An image edited by one user could also be spread to another for further editing, and this process can repeat several rounds. Hence, we need to ensure our watermarks can resist continual editing. As shown in Figure 6, we observe that the watermark embedded into the original image can be accurately extracted even after 3 editing rounds, demonstrating the watermark’s strong robustness against continual editing.

4.4. More Analysis

Relationship between editing strength and extraction ability. We explore the impact of the image editing strength (quantified by PSNR and SSIM computed between I_{wm} and I_{wm}^{edit}) on the extraction BER. As shown in Figure 8, points with higher BER are mainly at the area where PSNR and SSIM are low, *i.e.*, the editing strength is large. This is intuitive as the greater the change is, the more difficult it will be for the watermark extraction. When the editing strength on the original image is significant, the resulting edited image can be considered as a form of re-creation. In such cases, the risk of copyright infringement is relatively low, and the ineffective extraction may be deemed acceptable.

Relationship between the number of sampling steps and extraction ability. We test the BER of generated images at different sampling steps. Figure 7 (a) indicates that the model focuses on generating contours and layout at the first

λ_1	BER(%)\downarrow	PSNR\uparrow	SSIM\uparrow
0	1.7391	39.6859	0.9750
0.001	2.6579	41.9142	0.9910
0.01	6.0690	41.7604	0.9938
0.1	50.0364	56.9096	0.9986

Table 5. The impact of different λ_1 values. The gray cell denotes the default setting (same for the following tables).

few sampling steps, and then optimizing image details at later steps. As shown in Figure 7 (b), the BER decreases with more sampling steps.

Embedding mode of Robust-Wide. Figure 9 displays the normalized residual image between the watermarked and original images, using different watermarking methods. We can see that the watermarks embedded using DWT-DCT and DWT-DCT-SVD are quite faint and imperceptible, indicating their limited robustness. MBRS tends to concentrate primarily along the object’s edge contours, making it vulnerable to changes in the image background. In contrast, RivaGAN and our Robust-Wide embed watermarks in both the edges and backgrounds, resulting in enhanced robustness. Furthermore, we use Discrete Cosine Transform (DCT) and Discrete Fourier Transform (DFT) to visualize the residual images in the frequency domain. Watermarks embedded by DWT-DCT and DWT-DCT-SVD appear relatively uniform and weak. RivaGAN predominantly places watermarks in the low-frequency information areas, while MBRS distribute watermark information uniformly in the frequency domain. In contrast, Robust-Wide focuses on embedding watermarks in both low and high-frequency information regions, potentially making it more robust against semantically and conceptually related image modifications.

Extracting mode of Robust-Wide. We use the original image I_{ori} and watermarked image I_{wm} to generate the corresponding edited images I_{ori}^{edit} and I_{wm}^{edit} . Here, we control all potential random factors (*e.g.*, generation random seed) to guarantee that the difference between I_{ori}^{edit} and I_{wm}^{edit} is solely caused by instruction-driven image editing. As shown in Figure 10, the watermark embedded into the original image also exists after editing, which preserves as an outline of the character. We hypothesize that the extractor mainly focuses on such robust concept-aware areas.

4.5. Ablation Study

Impact of hyper-parameters λ_1 and λ_2 . Table 5 shows the watermark performance with different λ_1 values. We observe that a larger λ_1 can help improve the visual quality of watermarked images but causes a decrease in the watermark extraction rate. Table 6 shows the results with different λ_2 values. A higher λ_2 leads to lower BER, which showcases

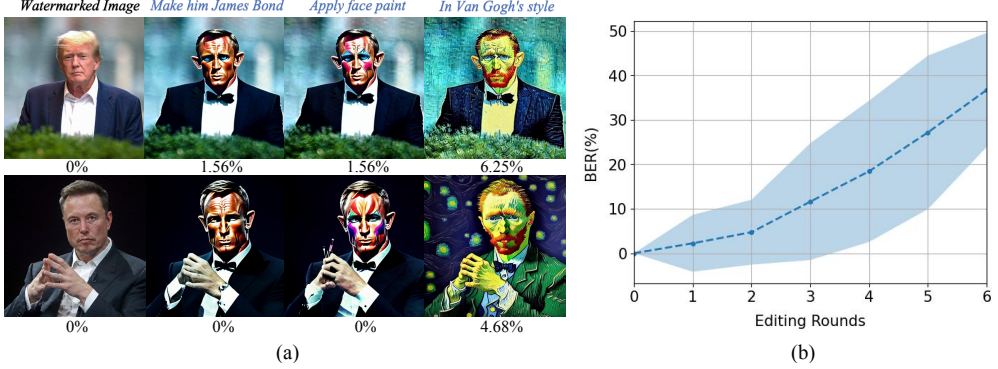


Figure 6. The influence of continual editing. (a) Some visual examples under continual editing (from left to right). (b) BER increases with more editing rounds. This experiment is conducted on real-world images as mentioned above.

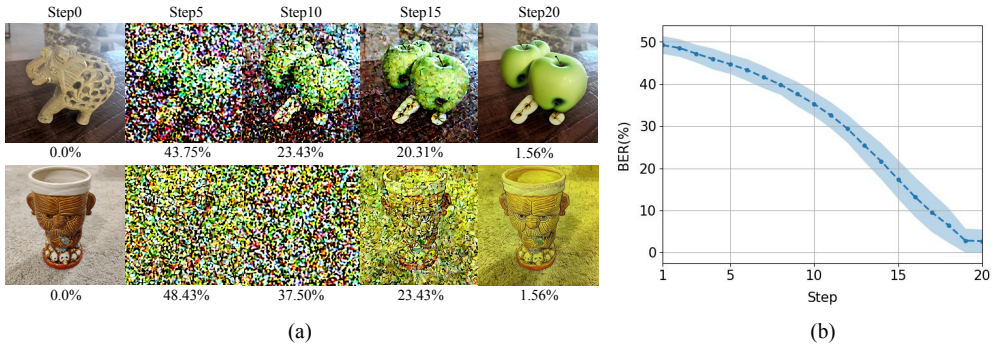


Figure 7. The influence of the number of sampling steps. (a) Some visual examples at different steps and their corresponding BER. (b) BER decreases with more sampling steps.

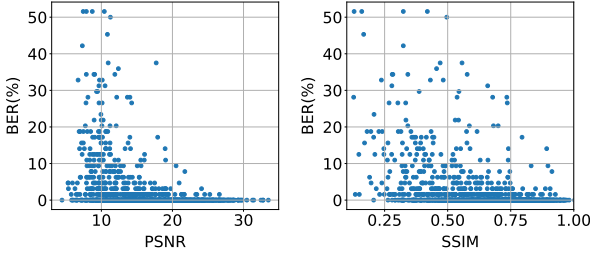


Figure 8. Scatter plots to show the relationship between the image editing strength and watermark extraction rate.

λ_2	BER(%)\downarrow	PSNR\uparrow	SSIM\uparrow
1	0.9674	35.2577	0.9616
0.1	2.6579	41.9142	0.9910
0.01	11.1796	45.8701	0.9929

Table 6. The impact of different λ_2 .

the trade-off between extraction ability and visual quality.

Importance of L_{ex_2} . With L_{ex_2} , the embedding network

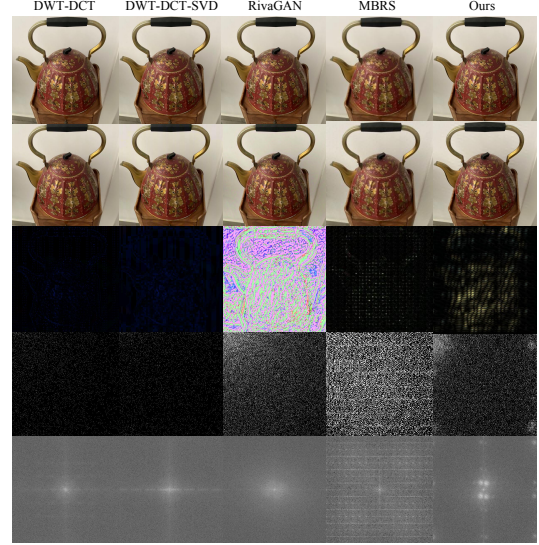


Figure 9. The embedding mode of different methods. From top to bottom: original images, watermarked images, normalized residual images, DCT and DFT of residual images, respectively

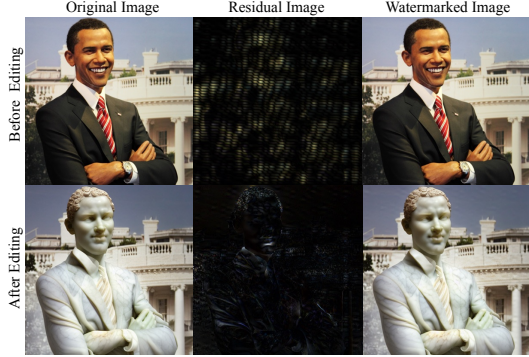


Figure 10. The impact of editing on the normalized residual image.

L_{ex_2}	BER(%) \downarrow		PSNR \uparrow	SSIM \uparrow
	w/o Editing	w/ Editing		
w/o.	50.1098	50.1219	68.7220	0.9999
w/.	0.0000	2.6579	41.9142	0.9910

Table 7. The importance of L_{ex_2} .

# of Gradient Backward Steps	BER(%) \downarrow	PSNR \uparrow	SSIM \uparrow
1	4.0520	44.3330	0.9938
2	2.9166	42.1386	0.9919
3	2.6579	41.9142	0.9910

Table 8. The influence of the number of gradient backward steps.

and extracting network tend to find desirable watermarking areas at first and then search more robust areas to resist instruction-driven image editing. Without L_{ex_2} , it is challenging to achieve watermark embedding and extraction only with edited images. Table 7 compares the performance under these two settings. The embedded watermark cannot be effectively extracted without L_{ex_2} , both before and after editing, with the BER of around 50%. Hence, L_{ex_2} is essential for the overall effectiveness of Robust-Wide.

Influence of the number of gradient backward steps k . Table 8 shows the watermark performance with different numbers of gradient backward steps. With more steps, the watermark message is easier to extract while the visual quality of the watermarked image slightly reduces. Due to the GPU memory constraints, the maximum number of gradient backward steps we could set is 3, which is sufficient to obtain acceptable performance.

Influence of different watermark lengths. Table 9 reports the evaluation results with different lengths of watermark messages. A longer watermark message results in higher BER and lower visual quality. In practice, the user can customarily select the watermark lengths to balance such

Watermark lengths (bits)	BER(%) \downarrow	PSNR \uparrow	SSIM \uparrow
16	2.2812	40.8327	0.9853
64	2.6579	41.9142	0.9910
256	4.1867	39.1842	0.9844
1024	6.3036	36.5956	0.9732

Table 9. The influence of different watermark message lengths.

trade-off. In Table 9, we can observe that the visual quality is lower when the watermark length is 16 compared to when the watermark length is 64. Indeed, the integration of watermark bit with the image involves shape transformations through convolutional or deconvolutional layers. With 16 bits, our available GPU memory posed restrictions on employing convolutional or deconvolutional layers for shape transformations. Consequently, we opted for a non-parametric interpolation method to handle the integration, causing degradation in visual quality.

5. Conclusion

In this paper, we propose Robust-Wide, the first robust watermarking methodology against instruction-driven image editing. Our core idea is to integrate a novel Partial Instruction-driven Denoising Sampling Guidance (*PIDSG*) module into the encoder-decoder training framework. Experiments demonstrate that Robust-Wide is robust against instruction-driven image editing in different scenarios while maintaining high visual quality and editability. Our in-depth analysis on the embedding and extracting modes of Robust-Wide is expected to shed light on the design of watermarking against other semantic distortions.

References

- [1] Alexander Quinn Nichol, Prafulla Dhariwal, Aditya Ramesh, Pranav Shyam, Pamela Mishkin, Bob McGrew, Ilya Sutskever, and Mark Chen. GLIDE: Towards photorealistic image generation and editing with text-guided diffusion models. In Kamalika Chaudhuri, Stefanie Jegelka, Le Song, Csaba Szepesvari, Gang Niu, and Sivan Sabato, editors, *Proceedings of the 39th International Conference on Machine Learning*, volume 162 of *Proceedings of Machine Learning Research*, pages 16784–16804. PMLR, 17–23 Jul 2022. [1](#), [2](#)
- [2] Aditya Ramesh, Prafulla Dhariwal, Alex Nichol, Casey Chu, and Mark Chen. Hierarchical text-conditional image generation with clip latents, 2022. [1](#), [2](#)
- [3] Chitwan Saharia, William Chan, Saurabh Saxena, Lala Li, Jay Whang, Emily L Denton, Kamyar Ghasemipour, Raphael Gontijo Lopes, Burcu Karagol Ayan, Tim Salimans, Jonathan Ho, David J Fleet, and Mohammad Norouzi. Photorealistic text-to-image diffusion models with deep language understanding. In S. Koyejo, S. Mohamed, A. Agarwal, D. Belgrave, K. Cho, and A. Oh, editors, *Advances in*

Neural Information Processing Systems, volume 35, pages 36479–36494. Curran Associates, Inc., 2022. 1, 2

[4] Robin Rombach, Andreas Blattmann, Dominik Lorenz, Patrick Esser, and Björn Ommer. High-resolution image synthesis with latent diffusion models. In *Proceedings of the IEEE/CVF conference on computer vision and pattern recognition*, pages 10684–10695, 2022. 1, 2

[5] Tim Brooks, Aleksander Holynski, and Alexei A. Efros. Instructpix2pix: Learning to follow image editing instructions. In *Proceedings of the IEEE/CVF Conference on Computer Vision and Pattern Recognition (CVPR)*, pages 18392–18402, June 2023. 1, 2, 4

[6] Tom Brown, Benjamin Mann, Nick Ryder, Melanie Subbiah, Jared D Kaplan, Prafulla Dhariwal, Arvind Neelakantan, Pranav Shyam, Girish Sastry, Amanda Askell, Sandhini Agarwal, Ariel Herbert-Voss, Gretchen Krueger, Tom Henighan, Rewon Child, Aditya Ramesh, Daniel Ziegler, Jeffrey Wu, Clemens Winter, Chris Hesse, Mark Chen, Eric Sigler, Mateusz Litwin, Scott Gray, Benjamin Chess, Jack Clark, Christopher Berner, Sam McCandlish, Alec Radford, Ilya Sutskever, and Dario Amodei. Language models are few-shot learners. In H. Larochelle, M. Ranzato, R. Hadsell, M.F. Balcan, and H. Lin, editors, *Advances in Neural Information Processing Systems*, volume 33, pages 1877–1901. Curran Associates, Inc., 2020. 1, 2

[7] Amir Hertz, Ron Mokady, Jay Tenenbaum, Kfir Aberman, Yael Pritch, and Daniel Cohen-or. Prompt-to-prompt image editing with cross-attention control. In *The Eleventh International Conference on Learning Representations*, 2022. 1, 2

[8] Shu Zhang, Xinyi Yang, Yihao Feng, Can Qin, Chia-Chih Chen, Ning Yu, Zeyuan Chen, Huan Wang, Silvio Savarese, Stefano Ermon, Caiming Xiong, and Ran Xu. Hive: Harnessing human feedback for instructional visual editing, 2023. 1, 2

[9] Kai Zhang, Lingbo Mo, Wenhui Chen, Huan Sun, and Yu Su. Magicbrush: A manually annotated dataset for instruction-guided image editing. *arXiv preprint arXiv:2306.10012*, 2023. 1, 2

[10] Tsu-Jui Fu, Wenze Hu, Xianzhi Du, William Yang Wang, Yinfei Yang, and Zhe Gan. Guiding instruction-based image editing via multimodal large language models, 2023. 1, 2

[11] Rinon Gal, Yuval Alaluf, Yuval Atzmon, Or Patashnik, Amit Haim Bermano, Gal Chechik, and Daniel Cohen-or. An image is worth one word: Personalizing text-to-image generation using textual inversion. In *The Eleventh International Conference on Learning Representations*, 2022. 1

[12] Md Maklachur Rahman. A dwt, dct and svd based watermarking technique to protect the image piracy. *International Journal of Managing Public Sector Information and Communication Technologies*, 4(2):21, 2013. 1, 2, 3, 5

[13] Jiren Zhu, Russell Kaplan, Justin Johnson, and Li Fei-Fei. Hidden: Hiding data with deep networks. In *Proceedings of the European Conference on Computer Vision (ECCV)*, September 2018. 1, 2

[14] ZhaoYang Jia, Han Fang, and Weiming Zhang. MBRS: Enhancing robustness of DNN-based watermarking by mini-batch of real and simulated JPEG compression. In *Proceedings of the 29th ACM International Conference on Multimedia*. ACM, oct 2021. 1, 3, 4, 5

[15] Matthew Tancik, Ben Mildenhall, and Ren Ng. Stegastamp: Invisible hyperlinks in physical photographs. In *Proceedings of the IEEE/CVF conference on computer vision and pattern recognition*, pages 2117–2126, 2020. 1, 3

[16] Han Fang and et al. Pimog: An effective screen-shooting noise-layer simulation for deep-learning-based watermarking network. In *ACM MM*, pages 2267–2275, 2022. 1, 2, 3

[17] Jascha Sohl-Dickstein, Eric Weiss, Niru Maheswaranathan, and Surya Ganguli. Deep unsupervised learning using nonequilibrium thermodynamics. In Francis Bach and David Blei, editors, *Proceedings of the 32nd International Conference on Machine Learning*, volume 37 of *Proceedings of Machine Learning Research*, pages 2256–2265, Lille, France, 07–09 Jul 2015. PMLR. 2

[18] Jonathan Ho, Ajay Jain, and Pieter Abbeel. Denoising diffusion probabilistic models. In H. Larochelle, M. Ranzato, R. Hadsell, M.F. Balcan, and H. Lin, editors, *Advances in Neural Information Processing Systems*, volume 33, pages 6840–6851. Curran Associates, Inc., 2020. 2

[19] Lvmin Zhang, Anyi Rao, and Maneesh Agrawala. Adding conditional control to text-to-image diffusion models. In *Proceedings of the IEEE/CVF International Conference on Computer Vision*, pages 3836–3847, 2023. 2

[20] Kevin Alex Zhang, Lei Xu, Alfredo Cuesta-Infante, and Kalyan Veeramachaneni. Robust invisible video watermarking with attention. 2019. 3, 4, 5

[21] Eric Wengrowski and Kristin Dana. Light field messaging with deep photographic steganography. In *Proceedings of the IEEE/CVF conference on computer vision and pattern recognition*, pages 1515–1524, 2019. 3

[22] Jun Jia, Zhongpai Gao, Kang Chen, Menghan Hu, Xiongkuo Min, Guangtao Zhai, and Xiaokang Yang. Rihoop: Robust invisible hyperlinks in offline and online photographs. *IEEE Transactions on Cybernetics*, 52(7):7094–7106, 2020. 3

[23] SD invisible watermark. <https://github.com/ShieldMnt/invisible-watermark>. 3

[24] Olaf Ronneberger, Philipp Fischer, and Thomas Brox. U-net: Convolutional networks for biomedical image segmentation. In *Medical Image Computing and Computer-Assisted Intervention–MICCAI 2015: 18th International Conference, Munich, Germany, October 5–9, 2015, Proceedings, Part III* 18, pages 234–241. Springer, 2015. 3, 4

[25] Patrick Esser, Robin Rombach, and Björn Ommer. Taming transformers for high-resolution image synthesis. In *Proceedings of the IEEE/CVF conference on computer vision and pattern recognition*, pages 12873–12883, 2021. 4

[26] Alec Radford, Jong Wook Kim, Chris Hallacy, Aditya Ramesh, Gabriel Goh, Sandhini Agarwal, Girish Sastry, Amanda Askell, Pamela Mishkin, Jack Clark, et al. Learning transferable visual models from natural language supervision. In *International conference on machine learning*, pages 8748–8763. PMLR, 2021. 4

- [27] Md. Maklachur Rahman. A DWT, DCT and SVD based watermarking technique to protect the image piracy. *International Journal of Managing Public Sector Information and Communication Technologies*, 4(2):21–32, jun 2013. 4
- [28] Xinyu Li. Diffwa: Diffusion models for watermark attack, 2023. 6
- [29] Chenlin Meng, Yutong He, Yang Song, Jiaming Song, Jiajun Wu, Jun-Yan Zhu, and Stefano Ermon. SDEdit: Guided image synthesis and editing with stochastic differential equations. In *International Conference on Learning Representations*, 2022. 6
- [30] Ron Mokady, Amir Hertz, Kfir Aberman, Yael Pritch, and Daniel Cohen-Or. Null-text inversion for editing real images using guided diffusion models. In *Proceedings of the IEEE/CVF Conference on Computer Vision and Pattern Recognition (CVPR)*, pages 6038–6047, June 2023. 7

A. Real-World Images Dataset

Here, we present a comprehensive overview of the construction process for the real-world images dataset. To encompass a diverse range of image modifications reflecting real-world scenarios, we opted for six categories of images from the Internet: person, animal, object, architecture, painting, and scenery. For each type, we chose five images and designed six hand-crafted editing instructions, respectively. More details are provided in the following part.

A.1. Real-World Images of Different Types

We show real-world images of different types in Figure 11.

A.2. Hand-crafted Editing Instructions

We show the designed editing instructions for each type.

Animal

“Move it to the desert”

“Put on a pair of sunglasses”

“Make it a cartoon”

“Make it in Van Gogh’s artistic style”

“Make it Picasso style”

“Make it Minecraft”

Architecture

“Make it an Egyptian sculpture”

“Turn it into ruins”

“Put it on fire”

“Make it Picasso style”

“Make it in Van Gogh’s artistic style”

“Make it Minecraft”

Object

“Replace it with an apple”

“Change it with a rose”

“Move it on the moon”

“Make it a Modigliani painting”

“Turn this into the space age”

“Make it Minecraft”

Painting

“Make it a Modigliani painting”

“Make it a Miro painting”

“Make it Picasso style”

“Make it a Van Gogh’s painting”

“Make it Minecraft”

“Make it a cartoon”

Person

“Apply face paint”

“Make it a zombie”

“Take off the clothes”

“Make it a marble roman sculpture”

“It should look 100 years old”

“Make it Minecraft”

Scenery

“Add a beautiful sunset”

“Cover it with snow”

“Make it a cyberpunk painting”

“Make it a Van Gogh’s painting”

“Make it Minecraft”

“Make it a pencil drawing”

B. More Visual Examples

B.1. Main Results.

See Figure 12.

B.2. Robustness Against Different Instruction-driven Image Editing Methods.

See Figure 13.

B.3. Robust-Wide’s Extracting Mode.

See Figure 14.

C. Code

Our code will be released upon acceptance.

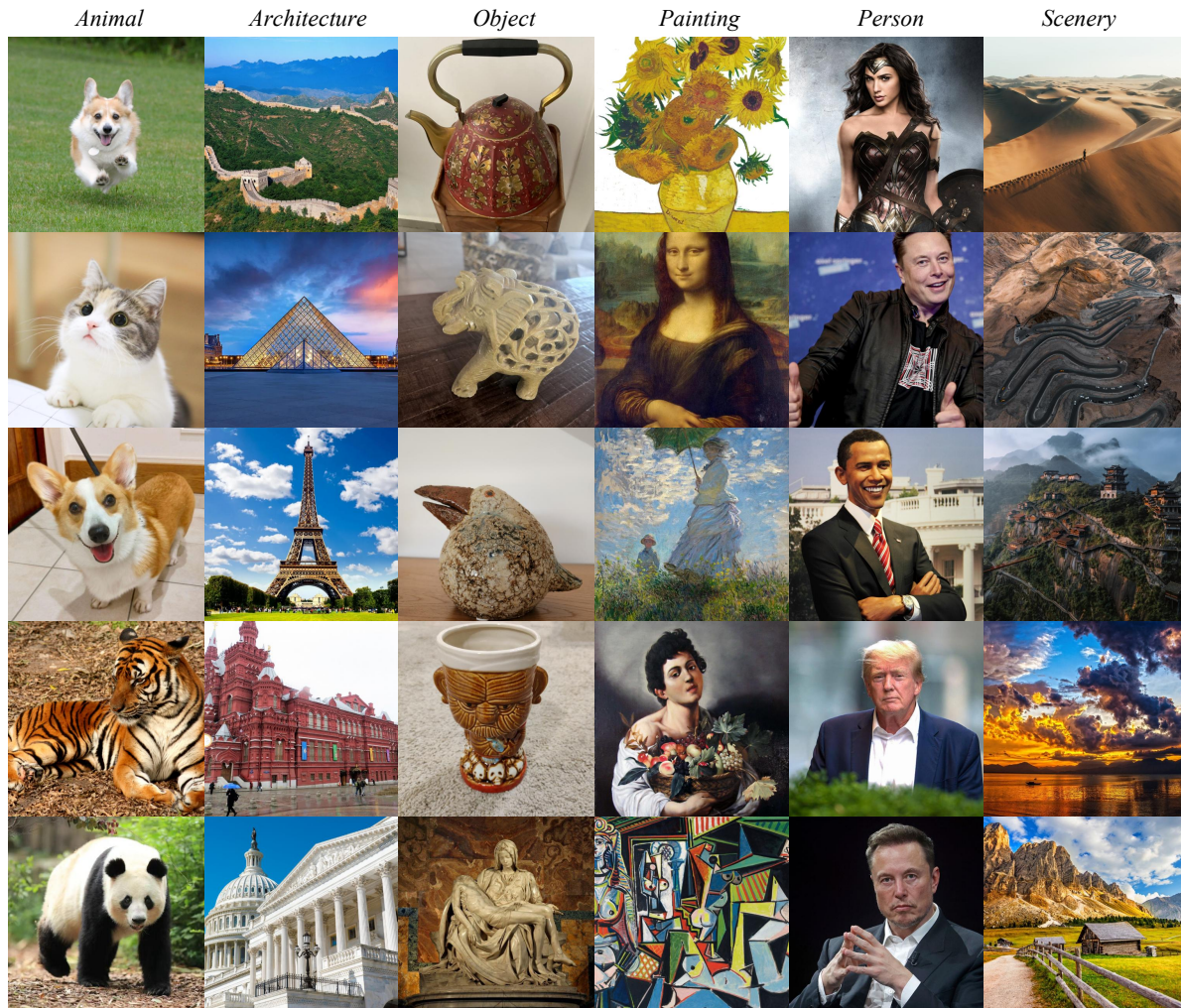


Figure 11. The real-world images of six types.

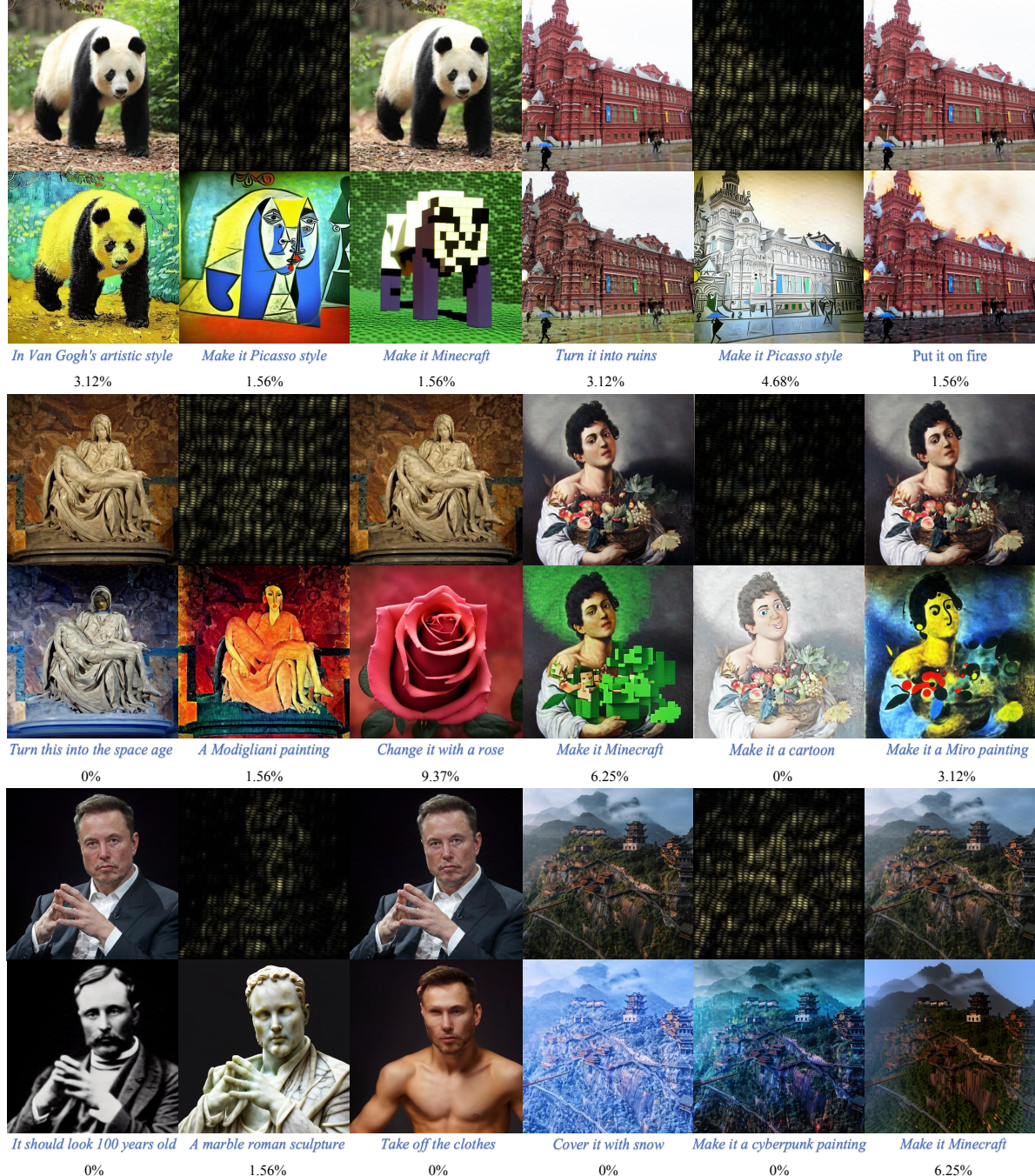


Figure 12. More visual examples from real-world images of six types, namely, animal, architecture, object, painting, person, and scenery. For each, the first row shows Original, Normalized Residual, and Watermarked Images and the second row shows Edited Images with the corresponding instructions, while BER is noted below.

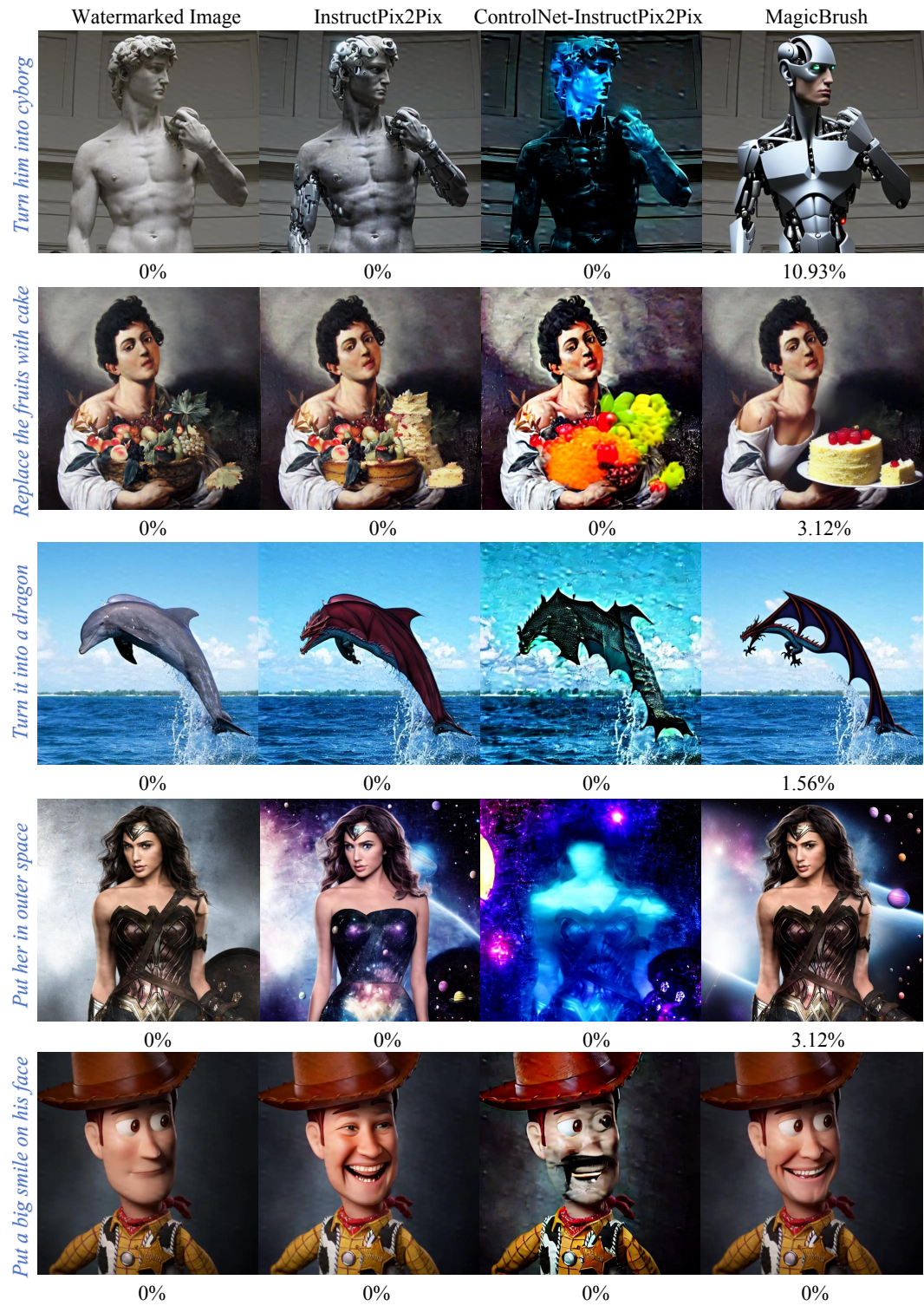


Figure 13. More visual examples of our robustness against different instruction-driven image editing methods.

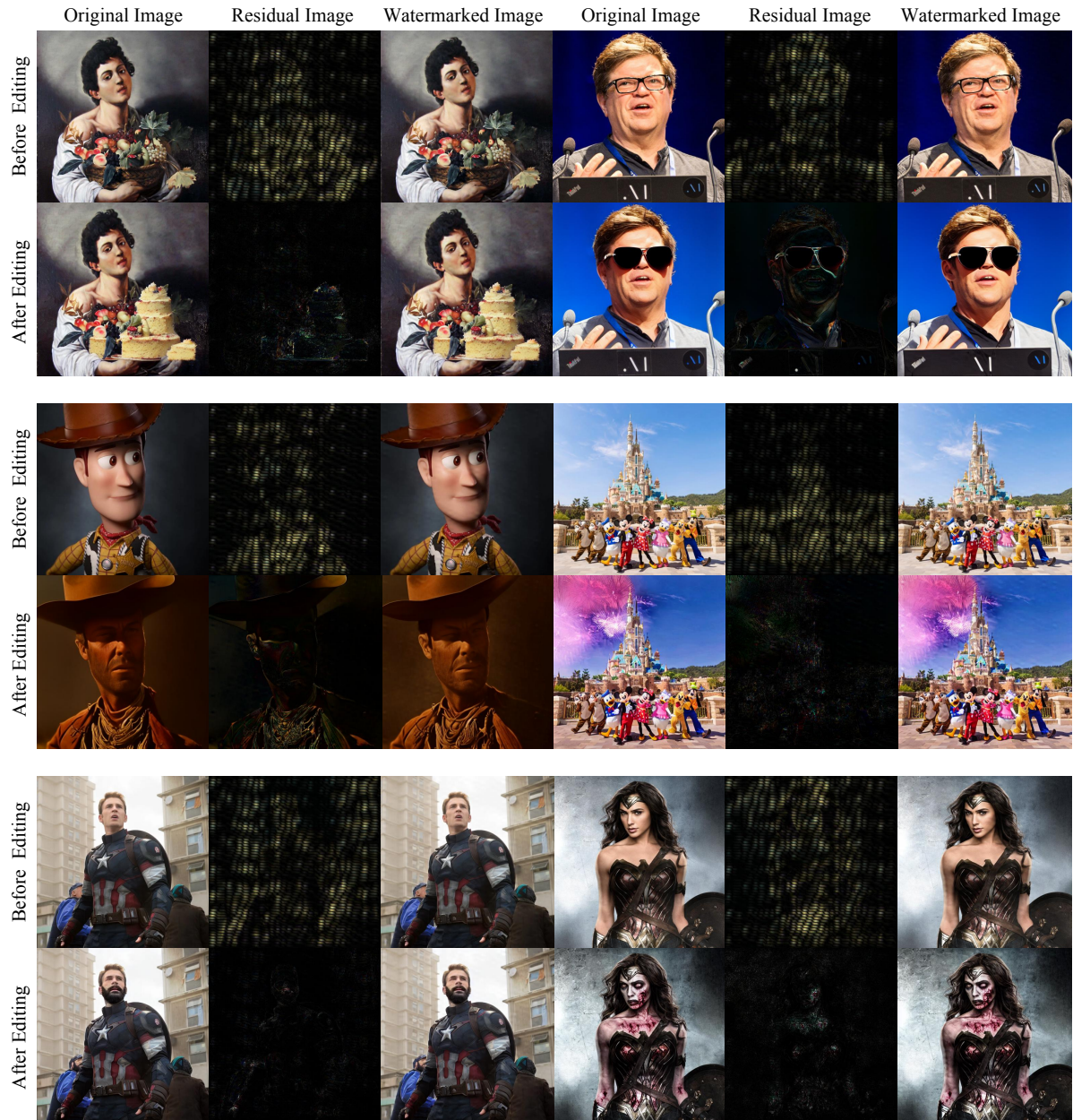


Figure 14. More visual examples of Robust-Wide's extracting mode.